INTERNATIONAL JOURNAL OF INTEGRATED ENGINEERING
ISSN: 2229-838X e-ISSN: 2600-7916

IJIE

Vol. 16 No. 1 (2024) 378-393
https://publisher.uthm.edu.my/ojs/index.php/ijie

Assessment of Agricultural Drought Using the Normalized Difference Drought Index (NDDI) to Prediction Drought at Corong River Basin

N. A. Affandy[1,4]*, D. Iranata[1], N. Anwar[1], M. A. Maulana[1], D. D. Prastyo[2], W. Wardoyo[1], B. M. Sukojo[3]

[1] *Department of Civil Engineering/Faculty of Civil, Planning and Geo-Engineering, Sepuluh Nopember Institute of Technology, Surabaya, East Java, 60111, INDONESIA*
[2] *Department of Statistics/Faculty of Science and Data Analytics, Sepuluh Nopember Institute of Technology, Surabaya, East Java, 60111, INDONESIA*
[3] *Department of Geomatics Engineering/Faculty of Civil, Planning and Geo-Engineering, Sepuluh Nopember Institute of Technology, Surabaya, East Java, 60111, INDONESIA*
[4] *Department of Civil Engineering/Faculty of Engineering, Universitas Islam Lamongan, Lamongan, East Java, 60111, INDONESIA*

*Corresponding Author: nurazizah@unisla.ac.id
DOI: https://doi.org/10.30880/ijie.2024.16.01.032

Article Info

Received: 11 December 2023
Accepted: 14 April 2024
Available online: 1 June 2024

Keywords

NDVI, NDWI, NDDI, agricultural drought, SARIMA

Abstract

As a complex and widespread natural phenomenon, drought poses a significant threat to the agricultural sector, especially in developing countries, resulting in significant economic losses. Its close relationship with water resilience and crop production necessitates sophisticated monitoring approaches for agricultural drought. Leveraging satellite remote sensing technology and various data types such as multispectral, thermal infrared, and microwave, can monitors drought on a large scale. This technology provides a comprehensive perspective for timely and spatial data collection, facilitating monitoring vegetation in vast agricultural areas. The study focuses on developing an agricultural drought model from 2017 to 2021, using Landsat 8 imagery. The model integrates the Normalized Difference Vegetation Index (NDVI) and Normalized Difference Water Index (NDWI), resulting in the establishment of the Normalized Difference Drought Index (NDDI) method. To predict agricultural drought in the Corong River Basin, the study employs the Seasonal Autoregressive Integrated Moving Average (SARIMA) model. Findings reveal varying degrees of dryness in the Corong River Basin, with 77% categorized as Strong dry conditions, 1% as Dry, 0.3% as Moderate wetness, and 21.6% as wetness. Drought predominantly occurs between July and October, impacting approximately 78% of the total dry area and extending across almost the entire region. The SARIMA $(0,0,1)(3,0,0)^{12}$ model, with a MAPE value of 0.2399, emerges as the most effective for predicting agricultural drought. These forecasted results provide critical insights into the level of agricultural drought in the Corong River Basin and valuable information for drought mitigation strategies, especially in regulating the distribution of irrigation water.

1. Introduction

Here introduce the paper, and put a nomenclature if necessary, in a box with the same font size as the rest of the paper. The paragraphs continue from here and are only separated by headings, subheadings, images and formulae. The section headings are arranged by numbers, bold and 10.0 pt. Here follows further instructions for Drought is an extreme and recurring event that can damage agricultural production and cause water scarcity [1]. Drought leads to various physical issues, such as the inability of crops to grow properly (known as puso) [2], [3] and can also increase the likelihood of forest and land fires [4]. Drought can be classified into four types: meteorological, hydrological, agricultural, and socioeconomic [5]. Drought severity is influenced by various factors such as the area's intensity, duration, geographical extent, and socioeconomic status [6]. When rainfall in a particular region falls significantly below (by 25% or more) the long-term average, it is called a meteorological drought [7]. Drought can lead to hydrological drought, characterized by surface water depletion, causing low river flow and drying up lakes, rivers, and reservoirs [8], [9]. Eventually, this results in agricultural drought, where soil moisture is inadequate and causes severe plant stress and decreased agricultural productivity [10].

Drought in agriculture is a complex natural and global phenomenon that can cause significant economic losses, especially for developing countries. Agricultural drought is closely related to water resilience and crop production [11]. Agricultural drought usually refers to when soil moisture decreases and affects crop production or even leads to crop failure without explicitly referring to surface water resources [12]. As the importance of food security is increasingly recognized, much research has been done to develop methodologies for monitoring agricultural drought. Over the past few decades, many methods have been developed to study agricultural drought based on factors such as rainfall, soil moisture, temperature, vegetation indices, and other indicators [13]

Drought assessment through indices has changed over time [14]-[16]. Initially, indices such as the Vegetation Drought Response Index (TVDI) [17] and the Vegetation Temperature Condition Index (VTCI) [18]-[20], which were based on vegetation and temperature, were developed. However, these indices have since expanded to form a collection of indices utilized for drought assessment. This group of indicators, which depends on plant life, comprises the Moisture Stress Index (MSI) [21], Simple Ratio Water Index (SRWI) [22], Normalized Difference Water Index (NDWI) [23], Normalized Difference Drought Index (NDDI) [24], Land Surface Water Index (LSWI) [25], Vegetation Condition Index (VCI) [26]-[28], and the Severity of Drought Index (DSI) [29]-[31].

The advancement of remote sensing satellite technology has enabled researchers to use various types of remote sensing data, including multispectral, thermal infrared, or microwave data, to monitor droughts on a large scale [32], [33]. Satellite remote sensing offers a comprehensive view of the land and spatial context for measuring the impact of drought, making it a valuable source of timely and spatially continuous data that can facilitate monitoring vegetation dynamics in large areas [33]. The normalized difference vegetation index (NDVI) calculated from remote sensing images is a widely used indicator to monitor droughts. It separates vegetation from the background soil and provides valuable information about vegetation health [34], [35]. However, NDVI alone may not be sufficient to identify vegetation drought, as other factors like land cover changes and pest attacks can cause similar anomalies. Rainfall and soil moisture datasets from microwave satellite sensors have also been utilized to monitor droughts. Studies have shown that NDVI has a slow response to rainfall deficit [36], [37]. Conversely, the Normalized Difference Water Index (NDWI) uses both bands in the near-infrared region and is highly sensitive to rainfall [38].

Remote sensing technology has been widely used to monitor drought in Indonesia. However, the technology and methods used have not been reviewed at different study scales. This review would help identify the strengths and weaknesses of the methods used, allowing for improvements in future studies. Researchers have used remote sensing data to monitor drought in Indonesia based on the VHI index, using MODIS and TRMM images at the island and provincial scales [39]. Additionally, some researchers have used Landsat-8 images, vegetation indices, and machine learning to monitor drought at the provincial scale in Central Java and the district scale using the VHI and NDDI indices [40]-[42]. In a recent study, the analysis of drought in agricultural land was conducted using the NDDI method based on the use of NDVI and NDWI with data collection years in 2015 and 2019 in the Ciampel Regency [43].

The Normalized Difference Drought Index (NDDI) is a superior drought index for several reasons. Firstly, it measures plant and soil water levels, which is critical for assessing drought severity. Secondly, it provides a more accurate reflection of the impacts of rainfall and crops compared to other indices. Additionally, it effectively reduces noise from the atmosphere and vegetation, which is not the case for indices such as NDVI or NDWI. Lastly, the NDDI is solely on satellite data, eliminating the need for extra weather data. These benefits make the NDDI an excellent tool for accurately monitoring drought conditions and their impacts [44], [45].

Predicting drought is vital for assisting local governments in minimizing the effects of drought and managing water resources efficiently. One of the most used methods for drought prediction is time series forecasting, where past observations are analyzed to establish a model that describes the correlation among them. The time series is then projected into the future based on this model. The Markov chain approach creates an early warning system [46]. They adopted a non-homogeneous Markov chain formulation to obtain drought characteristics and assess

dry spells in two climatic regions in Virginia, USA, based on long-term PDSI records [47]. Another frequently used time series model is the AutoRegressive Integrated Moving Average (ARIMA) model [48], [49]. However, this linear model presumes the time series data is stationary and cannot capture irregularities and non-linearities in the data.

The primary benefit of the ARIMA forecasting model is that it only necessitates time series data. Therefore, the ARIMA model is primarily used for time series analysis on the shipment of goods and transportation demand [50]. ARIMA modelling has also been utilized for streamflow and inflow [51], [52] and power grids [49]. The SARIMA model can adequately describe time series that exhibit non-stationarity within and across seasons. If the estimated parameter is more significant than one, the forecast result will be larger than the observation, and with an increase in forecast steps, the forecast value gradually increases.

The SARIMA modelling approach has been recognized as a statistical method recommended for data collected over a long period. The primary aim of this study is to create a model for agricultural drought using remote sensing, with Landsat 8 imagery as the data source, and combining Normalized Difference Vegetation Index (NDVI) and normalised Difference Water Index (NDWI) algorithms to create the NDDI method. The analysis will be done for the time from 2017 to 2021. The next step is to use this model to forecast agricultural drought in the Corong River Basin. Seasonal Autoregressive Integrated Moving Average (SARIMA) models will be used based on the time series of drought monitoring results obtained from the Normalized Difference Drought Index (NDDI).

2. Methodology

2.1 Study Area

This study takes place in the Corong River Basin, part of the Bengawan Solo River Basin, covering 815,081 km^2. The Bengawan Solo River Basin is between 110^{o}18' and 112^o 45' east longitude and between 6^o 49' and 8^o 08' south latitude (Fig. 1). The Corong River Basin is responsible for supplying water to the Gondang Reservoir. The Gondang Reservoir, currently under construction, is designed to supply water to 7 field reservoirs for ten months, covering an area of 6,233 hectares during the dry season. During the rainy season, water is obtained from rainfall. Besides meeting irrigation needs, the Gondang Reservoir is also intended for domestic use and is being developed for fish farming and tourism. The reservoir has motorboats, parks, and animal cages [53].

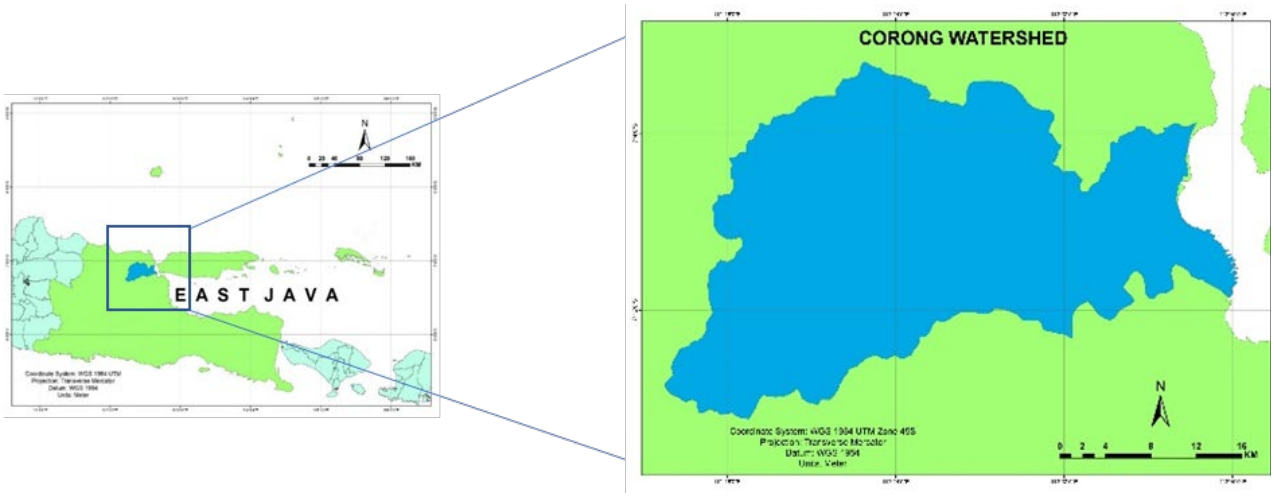

Fig. 1 *The location of the Corong River Basin*

2.2 The Normalized Difference Vegetation Index (NDVI)

The Normalized Difference Vegetation Index (NDVI) is the most used vegetation index for global greening. In green plants, chlorophyll substantially absorbs the Blue spectrum (0.4 - 0.5 m) and the Red spectrum (0.6 - 0.7 m) while reflecting the Green spectrum (0.5 - 0.6 m). As a result, healthy plants appear green. Between 0.7 and 1.3 µm, the Near Infrared (NIR) band of healthy plants has high reflectivity. The internal leaf structure of the plant primarily causes NDVI. Strong reflectance in the NIR spectrum and strong absorption in the red spectrum are both bands used to compute NDVI. The formula below provides the Normalized Difference Vegetation Index (NDVI).

$$NDVI = \frac{(\rho NIR - \rho \mathrm{Re}\, d)}{(\rho NIR + \rho \mathrm{Re}\, d)} \quad (1)$$

In this research analysis, Landsat 8 data was used to obtain NDVI values using the formula:

$$NDVI = \frac{(Band5 - Band4)}{(Band5 + Band4)} \quad (2)$$

NDVI is a classic index that measures vegetation growth and density, and ranges from -1.0 to 1.0. Negative values indicate clouds or water, while positive values indicate bare soil (values close to zero) and dense green vegetation (values equal to or greater than 0.4). NDVI is widely used to evaluate key vegetation parameters primarily influenced by climate conditions, human activities, and anthropogenic causes.
Generally, the following results were obtained: NDVI values ranging from -1 to 0 represent bodies of water. NDVI values ranging from -0.1 to 0.1 represent barren rock, sand, or snow. NDVI values ranging from 0.2 to 0.5 represent shrubs, grasslands, or mature plants. NDVI values ranging from 0.6 to 1.0 represent dense vegetation or tropical rainforests.

2.3 The Normalized Difference Water Index (NDWI)

The Normalized Difference Water Index (NDWI) is utilized to analyze water bodies, which involves using the remote sensing bands of Near Infrared and Green. This index is based on the fact that liquid water bodies typically reflect more light in the Blue spectrum (0.4-0.5 m) as compared to Green and Red spectra. The reflection in the visible spectrum's blue region gives clear water a blue appearance. However, murky water has a higher reflectance in the visible spectrum due to no reflection in the Near Infrared (NIR) band. NDWI was introduced by Gao in 1996 to improve the detection of water-related features in a landscape. The index uses the Near Infrared (NIR) and Shortwave Infrared (SWIR) bands, and its calculation involves a specific formula.

$$NDWI = \frac{(\rho NIR - \rho SWIR)}{(\rho NIR + \rho SWIR)} \quad (3)$$

For Landsat 8 data,

$$NDWI = \frac{(Band5 - Band6)}{(Band5 + Band6)} \quad (4)$$

In this research, the NDWI transformation is employed to investigate its correlation with the possibility of drought. The study assumes that when the spectral value of the moisture index transformation of an object is low and indicated by the red-coloured spatial data index, the object is drier. Conversely, the object is wetter or more humid when the spectral value is high and indicated by the blue-coloured spatial index.

2.4 The Normalized Difference Drought Index (NDDI)

The NDDI (Normalized Difference Drought Index) transformation determines drought conditions in agricultural land. Previous research has indicated a relationship between vegetation and moisture indexes. The assumption used in this study is that high drought index values will occur when both the vegetation index and moisture index decrease. If this happens, drought conditions will occur in agricultural land.
NDDI is a drought index developed to identify drought conditions in agricultural land. NDDI combines vegetation information from NDVI and water information from NDWI to obtain a better indication of agricultural drought conditions than using vegetation indices alone [54]. The equation for the NDDI value is:

$$NDDI = \frac{NDVI - NDWI}{NDVI + NDWI} \quad (5)$$

NDVI represents the Normalized Difference Vegetation Index, while NDWI represents the Normalized Difference Wetness Index. The NDDI value, ranging from -1 to 1, serves as an indicator of drought conditions, with higher values indicating a more severe drought [55]. To evaluate the severity of drought, the occurrence of drought for each pixel was assessed by considering the NDDI classes [56], [57] that wet exceed 0.5. These classes correspond to wet (NDDI<0.5 Moderate Wet (NDDI 0.5–0.7), Dry (NDDI 0.7–1.0), and Strong Dry (NDDI>1.0).

Int. Journal of Integrated Engineering Vol. 16 No. 1 (2024) p. 378-393

2.5 Image Processing

Remote sensing image data analysis using Landsat 8 OLI/TIRS level 2 images that have been geometrically and radiometrically corrected from 2017 to 2021. This data is employed for drought analysis using NDVI and NDWI. Both indices are utilized to conduct NDDI analysis.

2.6 Seasonal Autoregressive Integrated Moving Average (SARIMA)

The process of developing a SARIMA model involves several steps. First, creating ACF and PACF plots is necessary, followed by building the model and estimating its parameters while ensuring their significance. Subsequently, evaluating whether the residuals are white noise to determine the appropriate model. Finally, selecting the most suitable model is advised.

Autocorrelation measures how a time series is related to itself at different lags. The autocorrelation function (ACF) coefficient [58], denoted by ρ_k, is used to compute autocorrelation.

$$r_k = \frac{\sum_{t=1}^{n-k}\left(Z_t - \overline{Z}\right)\left(Z_{t+k} - \overline{Z}\right)}{\sum_{t=1}^{n-k}\left(Z_t - \overline{Z}\right)^2} \tag{6}$$

where k is 0, 1, 2, ..., n, the r_k is autocorrelation coefficient at lag k, Z_t is observation data at the time of the t, and $\bar{Z}$ is average data of observations.

Partial autocorrelation measures the degree of kinship of the linear relationship between and when the influence of time lag 1, 2, ..., k-1 is considered separate. According to, the estimate of PACF is based on the autocorrelation coefficient in the Yule-Walker equation for k time lag, i.e. [57].

$$\rho_1 = \phi_{k1} + \phi_{k2}\rho_1 + \ldots + \phi_{kk}\rho_{k-1} \tag{7}$$

$$\rho_k = \phi_{k1}\rho_1 + \phi_{k2}\rho_{k-2} + \ldots + \phi_{kk} \tag{8}$$

So that the estimation of the PACF value is obtained as follows:

$$\phi_{kk} = \frac{\rho_k - \sum_{j=1}^{k-1}\phi_{k-1,j}\rho_{k-j}}{1 - \sum_{j=1}^{k-1}\phi_{k-1,j}\rho_j} \tag{9}$$

with ϕ_{kj} is $\phi_{k-1,j} - \phi_{kk}\phi_{k-1,j-k}$ for j = 1, 2, ..., k-1, where ϕ_{kk} is partial autocorrelation coefficient at lag k, ρ_k is autocorrelation coefficient on the suspected lag k with r_k, ρ_j is autocorrelation coefficient on the suspected lag j with r_j, and ρ_{k-j} are autocorrelation coefficient on lag (k-j) suspected with r_{k-j}.

Seasonal Autoregressive Integrated Moving Average (SARIMA) model is denoted as ARIMA (ρ, d, q)(P, D, Q)s, where (ρ, d, q) represent the orders of the autoregressive (AR), moving average (MA), and non-seasonal differencing components, respectively. In contrast, (P,D, Q) represent the orders of the seasonal AR, MA, and seasonal differencing components. The seasonal pattern in the time series is represented by s, the seasonal period. The general form of the ARIMA (ρ, d, q)(P, D, Q)s model equation is written as follows:

$$\phi_p(B)\Phi_p\left(B^2\right)(1-B)(1-B_s)^D Y_t = \theta_q(B)\Theta_Q(B_s)\varepsilon_t \tag{10}$$

with $\phi_p(B) = (1 - \phi_1 B - \phi_2 B^2 - \cdots - \phi_p B^p)$; $\theta_q(B) = (1 - \theta_1 B - \theta_2 B^2 - \cdots - \theta_p B^q)$; $\Phi_p(B_s) = (1 - \Phi_1 B^s - \Phi_2 B^{2s} - \cdots - \Phi_p B^{ps})$ and $\Theta_Q(B_s) = (1 - \Theta_1 B^s - \Theta_2 B^{2s} - \cdots - \Theta_p B^{Qs})$, where Y_t is the observation at time t, ϕ_p is the AR coefficient at order p, θ_q is the MA coefficient at order q, ΦP is the Seasonal AR coefficient at order P, Θ_Q is the Seasonal MA coefficient at order Q, $(1 - B)^d$ is the Non-seasonal differencing, $(1 - B)^s$ is the Seasonal differencing, D is the Seasonal differencing order, s is the Number of periods per season, ε_t is the Residual at time t and B is the Backshift operator.

In the SARIMA method, the data needs to be in a stationary state. Thus, the initial step involves testing the stationarity of the data. This involves checking the stationarity of the variance using the Box-Cox transformation and examining the stationarity of the mean through the Augmented Dickey-Fuller test [59]. If the data is non-stationary in terms of variance and mean, it can be made stationary by applying variance stabilization transformation and differencing. The next step is identifying an initial model by analyzing the autocorrelation function (ACF) and partial autocorrelation function (PACF) plots. Following that, the parameters of the formed

model are estimated by assessing the significance of the AR, MA, seasonal, and non-seasonal parameters (they should significantly deviate from zero). A diagnostic check is performed as the fourth step. It ensures that the errors adhere to a white noise process, indicating the absence of autocorrelation. This check involves examining the results of the Ljung-Box test (p-value > alpha = 0.05). Additionally, the errors should exhibit a normal distribution, which is assessed by reviewing the outcomes of the Kolmogorov-Smirnov test (p-value > alpha = 0.05) [60]. Finally, the best model is chosen by considering the model with the smallest mean square error (MS) or the smallest means square [61].

3. Results and Discussion

3.1 The Normalized Difference Vegetation Index (NDVI)

The NDVI (Normalized Difference Vegetation Index) in remote sensing indicates the relationship between spectral variability and vegetation changes in growth rate. Since the index is determined using normalization processes, NDVI values range between 0 and 1, indicating sensitivity to green vegetation even in areas with little vegetation cover. This index generally applies to regional and global vegetation evaluation studies and is related to plant structure and photosynthesis [62]. The results are NDVI data processing in the Corong River Basin range from 0.21 to 0.73, with an annual average of 0.47. The trend in NDVI values varies yearly, experiencing decreases and increases strongly related to rainfall conditions. The highest increase occurred in 2021, and the lowest decrease occurred in 2019 and 2020. The NDVI value was calculated using Landsat surface reflectance remote sensing images that have been corrected with 30 m × 30 m medium-resolution data. This data can represent the vegetation cover properties in a specific area. Choosing this resolution can improve the accuracy of the results according to the field conditions and enhance plant efficiency and hydrological models [63].

From Fig. 2, in a recent study, NDVI was found to provide accurate land mapping around irrigation areas at a regional scale to understand drought in the event of decreased rainfall [3]. Changes in rainfall patterns in a warmer climate will strongly affect the hydrological cycle of agricultural land. For the possible effects of NDVI values in the region, accurate knowledge of the regional geographic distribution of irrigation areas is needed [64]. In this study, NDVI data were collected on a time series/periodic basis for 5 years, from 2017-2021, to represent regional characteristics in the study area.

Int. Journal of Integrated Engineering Vol. 16 No. 1 (2024) p. 378-393

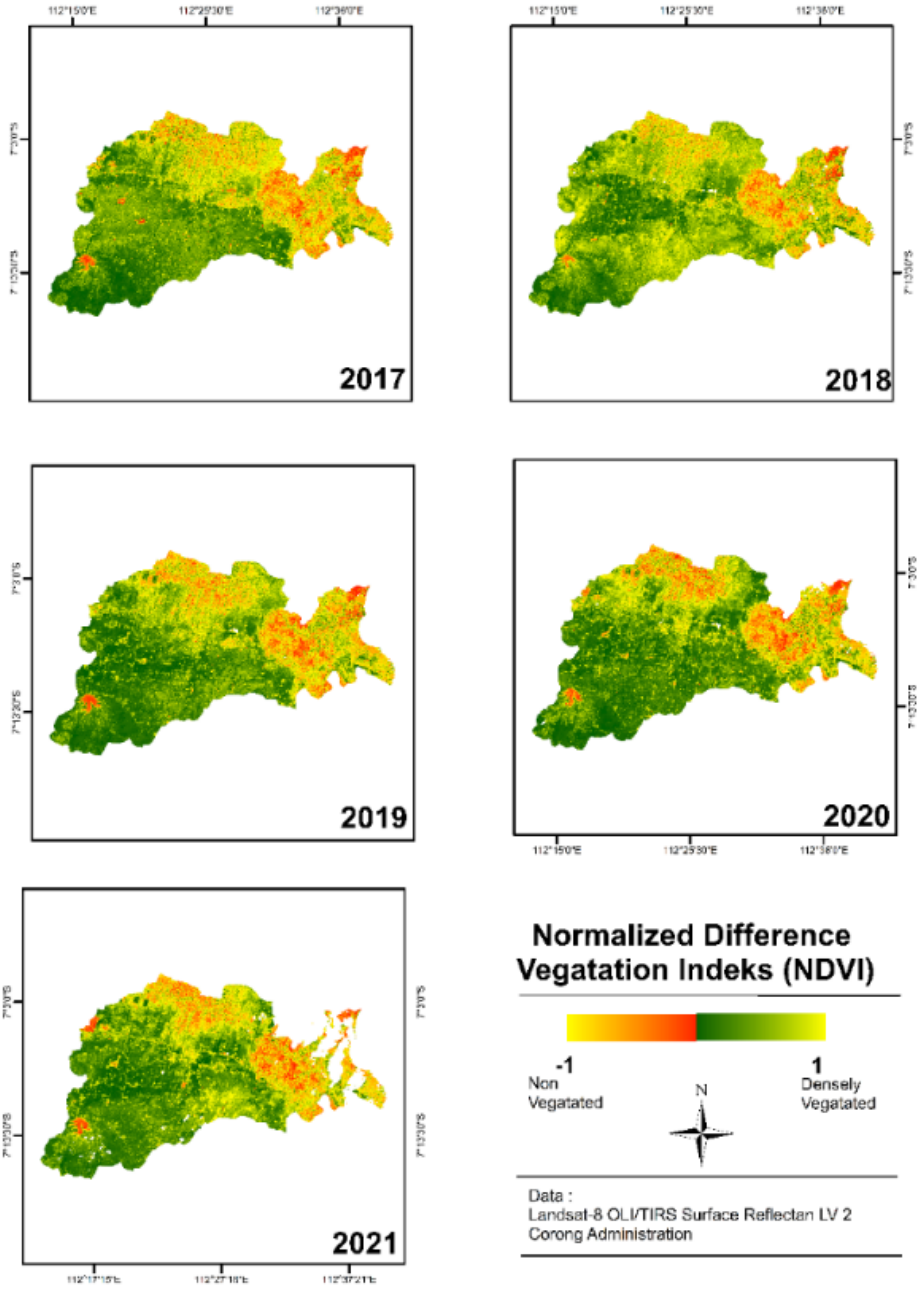

Fig. 2 *Map of NDVI distribution (2017-2021) in the Corong River Basin*

3.2 The Normalized Difference Water Index (NDWI)

NDWI is used in this research analysis to assess the reflection of water content in soil and on the surface of plants. The NDWI value ranges from -1 to +1, where higher NDWI values indicate a high plant water content. Lower NDWI values indicate a low vegetation water content, causing a decrease in NDWI during water absorption periods. At this point, it is often stated that NDWI can be used to determine the degree of wetness or dryness. When rainfall increases, the NDWI value also increases [5].

From Fig. 3, The results of NDVI data processing in the Corong River Basin are from -0.608 to -0.256, with an annual average of -0.506. The NDWI value in this area generally indicates a low level of wetness, even tending to be dry. Although there has not been a significant change in the NDWI value, this data can represent the water content in both soil and surface. The northern area has a relatively high level of wetness, while the central to southern areas are relatively dry. This finding is consistent with previous research [65], which shows that areas with high NDWI values have vegetation or soil with high water or moisture content, especially around the Gondang reservoir.

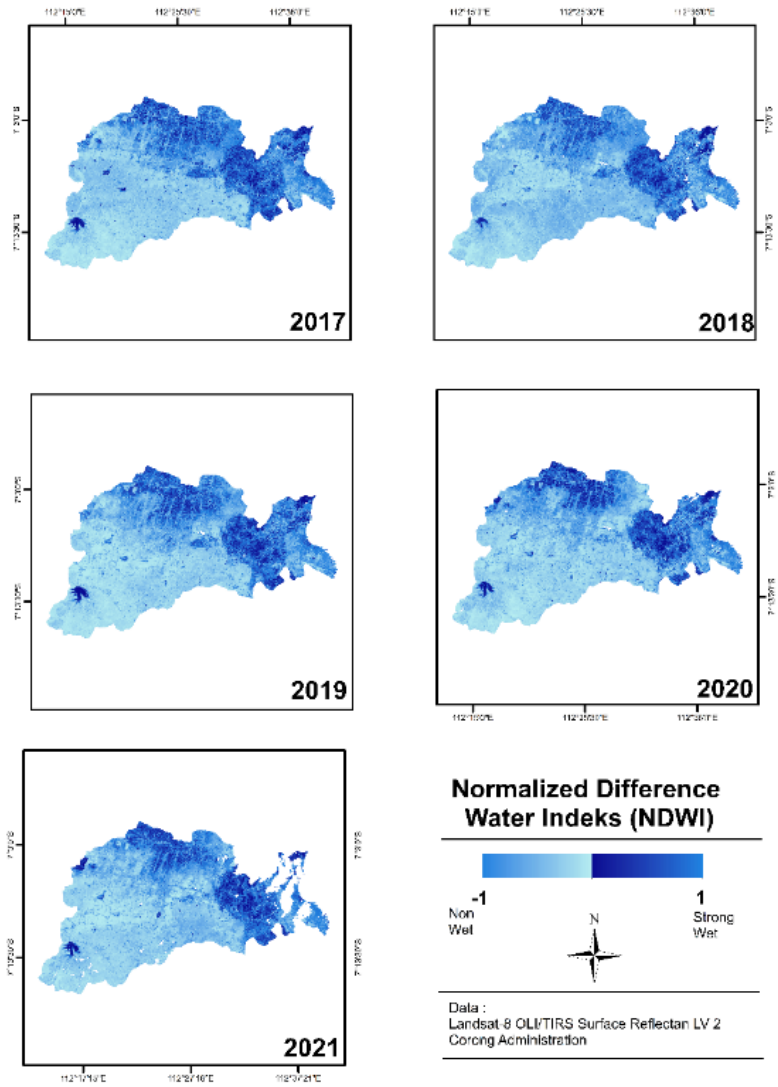

Fig. 3 *Map of NDWI distribution (2017-2021) in the Corong River Basin*

3.3 The Normalized Difference Drought Index (NDDI)

The NDDI transformation combines data from NDVI and NDWI to create a broader and more precise range of transformation values, with differences of up to 5%. NDVI uses radiation absorption to measure vegetation canopy chlorophyll and mesophyll content, while NDWI measures canopy moisture based on water and mesophyll content. In the NDDI transformation, higher values indicate denser and wetter vegetation. However, in the case of NDDI transformation, higher values imply drier areas.

NDDI can be classified into three classes: no drought (NDDI value less than 0.1), moderate drought (NDDI value ranging from 0.1 to 0.3), and severe drought (NDDI value greater than 0.3) (Fig. 4). However, some studies may use different thresholds or categories depending on context and purpose. This study measured drought with vulnerability index classes following the latest research conducted in Romania with characteristics of wheat farming areas. The drought classes were moderate drought (0.5 - 0.6), severe drought (0.6 - 1.0), and extreme drought (>1.0).

From Fig. 4, the study shows that the Corong River Basin experienced 77% Strong dry, 1% Dry, 0.3% Moderate wetness, and 21.6% wetness. The proportion of the area affected by drought has increased in the last two years, 2020 and 2021, while there was a significant decrease in 2018. Agriculture in the area is greatly affected by drought. Although NDVI analysis shows that vegetation such as rice grows in the area, NDWI analysis indicates that the area experiences drought due to low soil moisture levels.

Regular analyses are conducted to monitor the area's dryness level based on NDDI processing data. It is found that drought often occurs from July to October every year. The average percentage of dry areas is 78% of the total area during these months. In Fig. 5, the distribution of drought occurs in almost the entire area. In 2017, wetness only occurred in a few scattered points, while in most of the area, it was almost dry. In 2018, wetness increased in

Int. Journal of Integrated Engineering Vol. 16 No. 1 (2024) p. 378-393

the southern part of the area, while from 2019 to 2021, wetness only occurred in the northern to eastern regions, with a little in the south.

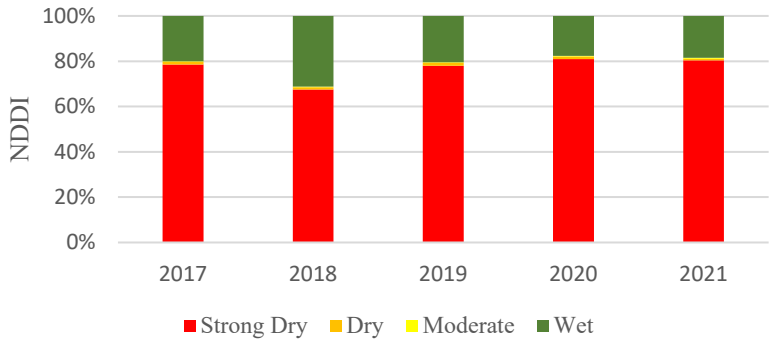

Fig. 4 *Map of NDWI distribution (2017-2021) in the Corong River Basin*

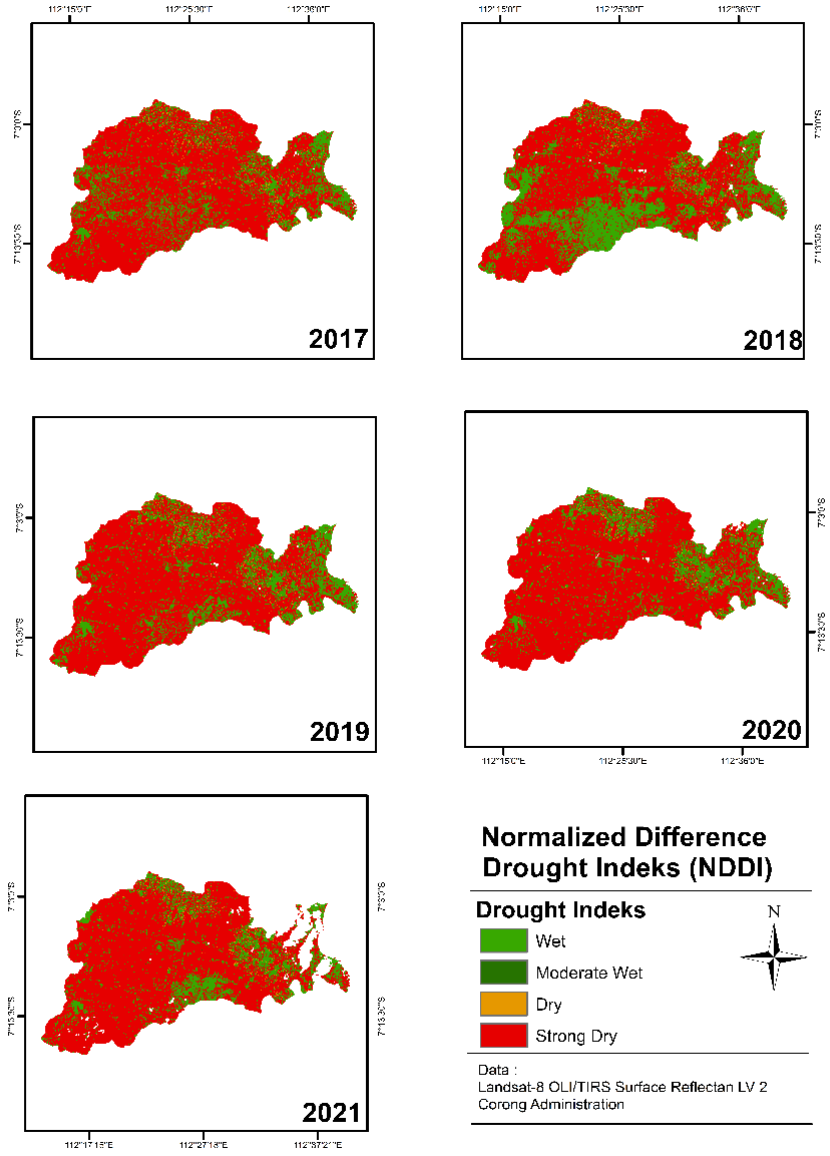

Fig. 5 *Map of NDDI distribution (2017-2021) in the Corong River Basin*

3.4 Forecasting Agricultural Drought using Normalized Difference Drought Index (NDDI) with Seasonal Autoregressive Integrated Moving Average (ARIMA)

3.4.1 Identification of Stationarity in Mean

After the data is declared stationary in variance, it will also be tested for stationarity in the mean. A stationarity test in the mean uses the Augmented Dickey-Fuller test. Based on the test results from Augmented Dickey-Fuller, a δ value of -3.87209 and a ρ-value of 0.002 were obtained. The data can be considered stationary in the mean, thus fulfilling the assumption of stationarity. They can be continued for further analysis: ARIMA modelling using ACF and PACF plots.

3.4.2 Identification of ARIMA Model Order

The model order of ARIMA can be determined using ACF and PACF plots. In Fig. 6, it is shown that the NDDI time series plot of the agricultural drought index in the Corong River Basin has an ACF lag 12, indicating that the differencing process is not necessary. For the PACF graph, a lag 12 outside the lines indicates seasonal data. From the above ACF and PACF tables, the tentative ARIMA model is ARIMA $(1,0,1)(3,0,2)^{12}$, ARIMA $(0,0,1)(3,0,0)^{12}$, ARIMA $(1,0,0)(0,0,2)^{12}$, ARIMA $(1,0,0)(0,0,1)^{12}$, and ARIMA $(0,0,2)(3,0,1)^{12}$.

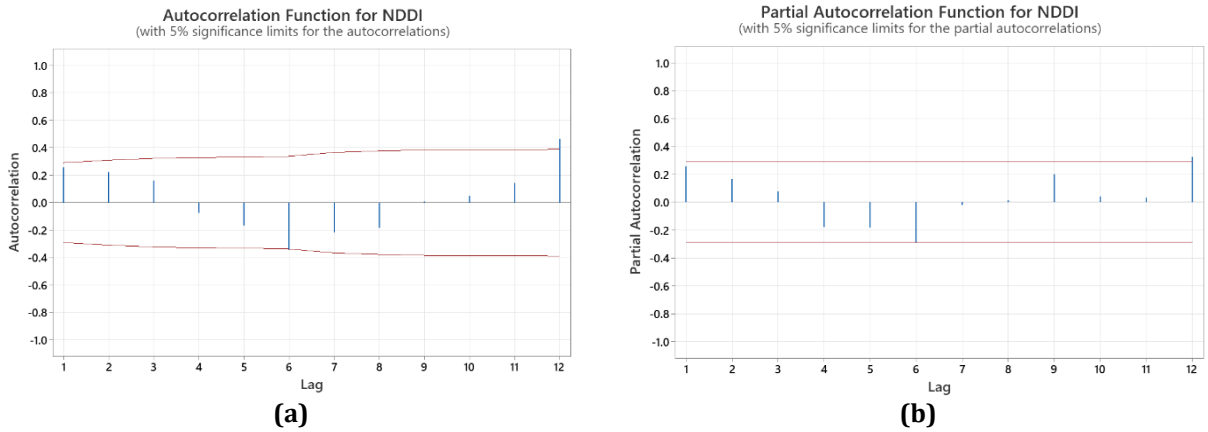

(a) **(b)**

Fig. 6 *A time series plot, (a) autocorrelation function (ACF), and (b) partial autocorrelation function (PACF) of the NDDI agricultural drought index in the Corong River Basin*

3.4.3 Parameter Significance Test

Once the ARIMA model has been estimated, the next step is to estimate the parameters of the ARIMA model and perform significance tests on them. The estimated parameters and their significance testing results for each model estimation are presented in Table 1. Based on the results, it can be seen that the significance test and parameter estimation results from the ARIMA model suggest that all models are significant.

Table 1 *Parameter significance test ARIMA model of NDDI*

Model	Estimation	ρ-value	**Significance of Parameters**
ARIMA $(1,0,1)(3,0,2)^{12}$	AR1	0.016	Significance
	SAR1	0.006	Significance
	SAR2	0.017	Significance
	SAR3	0.000	Significance
	MA1	0.000	Significance
	SMA1	0.000	Significance
	SMA2	0.041	Significance
ARIMA $(0,0,1)(3,0,0)^{12}$	SAR1	0.000	Significance
	SAR2	0.000	Significance
	SAR3	0.000	Significance
	MA1	0.000	Significance
ARIMA $(1,0,0)(0,0,2)^{12}$	AR1	0.000	Significance
	SMA1	0.004	Significance
	SMA2	0.014	Significance
ARIMA $(1,0,0)(0,0,1)^{12}$	AR1	0.000	Significance
	SMA1	0.003	Significance
ARIMA $(0,0,2)(3,0,1)^{12}$	SAR1	0.000	Significance
	SAR2	0.000	Significance
	SAR3	0.000	Significance
	MA1	0.000	Significance
	MA2	0.017	Significance

	SMA1	0.001	Significance

3.4.4 Diagnostic Test of Residuals

After the estimation and significance test of the parameters of the ARIMA model, an independent test of the model residuals will be conducted to determine whether there is any autocorrelation in the residual model or a white noise test. Based on the results from Table 2, it can be said that some of the estimated model residuals ARIMA (1,0,1)(3,0,2)12 and ARIMA (0,0,2)(3,0,1)12 have p-values < 0.05, indicating that the residual model is autocorrelated.

Table 2 *The significance test of parameters and the Ljung-box-pierce test of the tentative SARIMA model*

Model	*p-value*	Significance of Parameters
ARIMA $(1,0,1)(3,0,2)^{12}$	0.000	Non Significance
ARIMA $(0,0,1)(3,0,0)^{12}$	0.138	Significance
ARIMA $(1,0,0)(0,0,2)^{12}$	0.921	Significance
ARIMA $(1,0,0)(0,0,1)^{12}$	0.491	Significance
ARIMA $(0,0,2)(3,0,1)^{12}$	0.000	Non Significance

3.4.5 Selection of The Best Model

Next, the significant models that have undergone residual diagnostic testing will be evaluated for their AIC values, and the best model will be selected based on the criterion of the smallest AIC value. The following are the AIC values of the significant models. Table 3 and Fig. 7 show that the best model can be selected based on the smallest AIC. To make predictions, the best model with the smallest AIC is ARIMA $(0,0,1)(3,0,0)^{12}$.

Table 3 *The AIC value of the estimated model*

KODE	Model	*AIC*	MAPE
$SARIMA_1$	ARIMA $(0,0,1)(3,0,0)^{12}$	294,45	0.239947
$SARIMA_2$	ARIMA $(1,0,0)(0,0,2)^{12}$	321.31	0.526315
$SARIMA_3$	ARIMA $(1,0,0)(0,0,1)^{12}$	326.68	0.541836

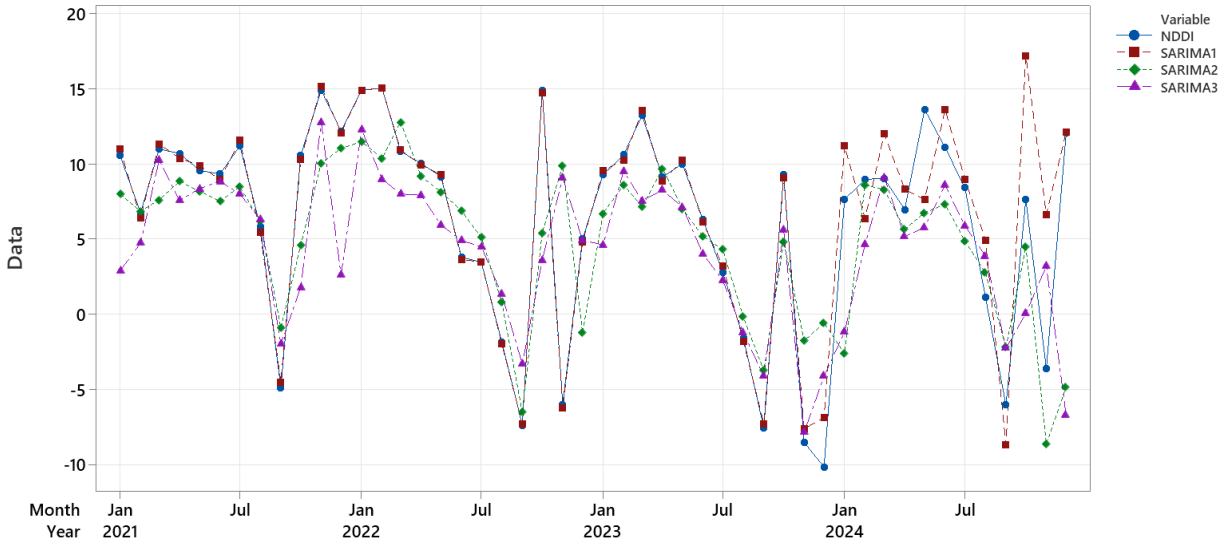

Fig. 7 *Time Series Plot NDDI, $ARIMA_1$, $ARIMA_2$ and $ARIMA_3$*

ARIMA $(0,0,1)(3,0,0)^{12}$ is a statistical model for analyzing time series data. The mathematical equation for this model is as follows:

$$\left(1-\Phi_1 B^s-\Phi_2 B^{2s}-\Phi_3 B^{3s}\right)Y_t=\left(1-\theta_1 B\right)\varepsilon_t \tag{11}$$

$$Y_t - \Phi_1 B^{12} Y_t - \Phi_2 B^{12} Y_t - \Phi_3 B^{12} Y_t = \varepsilon_t - \theta_1 B \varepsilon_t \quad (12)$$

$$Y_t + 0.6883 Y_{t-12} - 0.7068 Y_{t-24} - 0.9823 Y_{t-36} = \varepsilon_t + 1.01100 \varepsilon_{t-1} \quad (13)$$

where is the value of the time series at time t, c is a constant, ε_t is the noise at time t, θ_1 is an autoregressive moving average (ARMA) parameter, Φ_1, Φ_2, and Φ_3 are autoregressive seasonal (SAR) parameters with a period of 12, and (0,0,1) indicates that the model has one regular moving average (MA) parameter. This ARIMA model can be used to predict the value of Y_t in the future based on historical data that has been observed.

$$Y_t + 0.6883 Y_{t-12} - 0.7068 Y_{t-24} - 0.9823 Y_{t-36} = \varepsilon_t + 1.01100 \varepsilon_{t-1} \quad (14)$$

3.4.6 Prediction

If the best model has been obtained, ARIMA (0,0,1)(3,0,0)12, the next step is to make predictions for the next 12 months from January to December 2021, which can be seen in Table 4 with a MAPE value of 0.2399.

Table 4 *Results of NDDI using ARIMA (0,0,1)(3,0,0)[12]*

Period	Actual	Forecast	Category
Jan 2021	17.4120	15.8248	Strong dry
Feb 2021	11.2570	16.0686	Strong dry
Mar 2021	6.4850	13.7689	Strong dry
Apr2021	8.4680	11.4934	Strong dry
Mei 2021	10.4730	6.6635	Strong dry
Jun 2021	10.0780	0.5361	Moderate wet
Jul 2021	7.7190	-0.4273	wet
Aug 2021	1.6210	-3.7083	wet
Sep 2021	-5.0610	-8.4222	wet
Oct 2021	-2.7300	15.9137	Strong dry
Nov 2021	-3.8800	-9.4135	wet
Dec 2021	10.6710	-10.5355	wet

In Table 4, it can be seen that according to the model for forecasting, the highest drought value of 16.0686 was obtained in February 2021. However, from the actual data, the highest drought value of 17.4120 was obtained in January 2021. The Mean Squared Error value can be calculated as follows:

$$MSE = \frac{1}{n}\sum_{i=1}^{n}\left(Y_i^{'} - Y_i\right)^2 = \frac{1}{12}\left(1127.423\right) = 93.9519 \quad (15)$$

From the above analysis, the Mean Squared Error value obtained is 93.9519. The Mean Squared Error method is generally used to check the estimated error value in forecasting. A low Mean Squared Error value or a Mean Squared Error value close to zero indicates that the forecasted results align with the actual data and can be used for future forecasting calculations.

3.5 Discussion

This study aimed to create a model for agricultural drought using remote sensing, with Landsat 8 imagery as the data source, and combining Normalized Difference Vegetation Index (NDVI) and normalized Difference Water Index (NDWI) algorithms to create the NDDI method. This will be done for the time from 2017 to 2021. The next step is to use this model to forecast agricultural drought in the Corong River Basin. Seasonal Autoregressive Integrated Moving Average (ARIMA) models will be used based on the time series of drought monitoring results obtained from the Normalized Difference Drought Index (NDDI). The research revealed that the Corong watershed region suffered from 77% Strong dry, 1% Dry, 0.3% Moderate wetness, and 21.6% wetness. The percentage of drought-affected areas has increased in the last two years (2020-2021), whereas there was a significant decrease

in 2018. This rise is likely due to the El Nino and La Nina phenomena, which intensified in Indonesia in 2019-2020 and probably contributed to the increased percentage of dry areas. Regular assessments are performed based on NDDI data processing to track the region's dryness level [60]. The study also found that drought mainly occurred from July to October every year, with an average of 78% of the area being dry during these months. The distribution of drought covered nearly the entire region. In 2017, only a few scattered points had wetness, while the rest of the area was almost dry. Wetness increased in the southern part of the area in 2018, whereas from 2019 to 2021, wetness occurred primarily in the northern to eastern regions and, to a lesser extent, in the south. Based on the discussion results, the author concluded that the ARIMA (0,0,1)(3,0,0)12 model with a MAPE value of 0.2399 is suitable for predicting agricultural drought using NDDI based on the testing steps that have been carried out. This is because it is the model with the smallest AIC value, has significant parameters, and meets all assumptions. Based on the analysis provided, the calculated Mean Squared Error is 93.9519. The Mean Squared Error technique is commonly employed to assess the accuracy of forecasts by measuring the magnitude of estimation errors. A smaller Mean Squared Error value, or one that approaches zero, indicates a closer alignment between the forecasted values and the actual data, thus making it suitable for future forecasting calculations. Predictions were made for the following 12 periods using this model, showing the level of agricultural drought in the Corong River Basin. These results can be used for drought mitigation, especially for regulating water distribution in irrigation areas.

4. Conclusion

Based on the discussion results, the study found that the Corong River basin experienced a drought of 77% Strong dry, 1% Dry, 0.3% Moderate wetness, and 21.6% wetness. The study also found that drought mainly occurred from July to October each year, with an average of 78% of the total dry area during those months. The distribution of drought covers almost the entire area. Meanwhile, the best forecasting model for drought analysis was obtained using the ARIMA $(0,0,1)(3,0,0)^{12}$ model with a MAPE value of 0.2399, suitable for predicting agricultural drought using NDDI. This model was the best because it had the smallest AIC value and significant parameters and met all assumptions. The prediction results for the next 12 months can indicate the level of agricultural drought in the Corong River Basin, which can be used for drought mitigation, especially in regulating the distribution of irrigation water in dry seasons.

Acknowledgements

The authors gratefully acknowledge the contributions of the Ministry of Education and Culture of the Republic of Indonesia Through Education Scholarship Grants Domestic Postgraduate (BPPDN) and The Research and Development at the Islamic University of Lamongan. This work was supported by the Ministry of Education and Culture of the Republic of Indonesia and Internal Grants 2022 for Research and Development at the Islamic University of Lamongan.

Conflict of Interest

Authors declare that there is no conflict of interests regarding the publication of the paper.

Author Contribution

The authors confirm their contributions to the paper as follows: Authors Nur Azizah, Nadjadji Anwar, Wasis Wardoyo, and Data Iranata were responsible for the ***conception and design of the study****;* ***data collection*** *was carried out by Author Nur Azizah;* ***analysis and interpretation of the results*** *were conducted by Authors Nur Azizah, Mahendra Andiek, Dedy Dwi Prstyo, and Bangun Muljo S;* ***draft manuscript*** *preparation was done by Authors Nur Azizah and Bangun Muljo S. All authors reviewed the results and approved the final version of the manuscript.*

References

[1] Rosa, L., Chiarelli, D. D., Rulli, M. C., Dell'Angelo, J., & D'Odorico, P. (2020). Global agricultural economic water scarcity. Science Advances, 6(18), 1-10. https://doi.org/10.1126/sciadv.aaz6031

[2] Boer, R., & Subbiah, A. R. (2005). Agricultural Drought in Indonesia. In Monitoring and Predicting Agricultural Drought. Oxford University Press. https://doi.org/10.1093/oso/9780195162349.003.0037

[3] Surmaini, E., Hadi, T. W., Subagyono, K., & Puspito, N. T. (2015). Early detection of drought impact on rice paddies in Indonesia by means of Niño 3.4 index. Theoretical and Applied Climatology, 121(3–4), 669–684. https://doi.org/10.1007/s00704-014-1258-0

[4] Littell, J. S., Peterson, D. L., Riley, K. L., Liu, Y., & Luce, C. H. (2016). A review of the relationships between drought and forest fire in the United States. Global Change Biology, 22(7), 2353–2369. https://doi.org/10.1111/gcb.13275

[5] Harisuseno, D. (2020). Comparative study of meteorological and hydrological drought characteristics in the Pekalen River basin, East Java, Indonesia. Journal of Water and Land Development, Vol 45 (IV-VI), 19–41. https://doi.org/10.24425/jwld.2020.133043
[6] Wilhite, D. A., & Glantz, M. H. (1985). Understanding: The drought phenomenon: The role of definitions. Water International, 10(3), 111–120. https://doi.org/10.1080/02508068508686328
[7] Brito, C. S. de, Silva, R. M. da, Santos, C. A. G., Brasil Neto, R. M., & Coelho, V. H. R. (2021). Monitoring meteorological drought in a semiarid region using two long-term satellite-estimated rainfall datasets: A case study of the Piranhas River basin, northeastern Brazil. Atmospheric Research, 250, 105380. https://doi.org/10.1016/j.atmosres.2020.105380
[8] He, X., Wada, Y., Wanders, N., & Sheffield, J. (2017). Intensification of hydrological drought in California by human water management. Geophysical Research Letters, 44(4), 1777–1785. https://doi.org/10.1002/2016GL071665
[9] Pathak, A. A., Channaveerappa, & Dodamani, B. M. (2016). Comparison of two hydrological drought indices. Perspectives in Science, 8, 626–628. https://doi.org/10.1016/J.PISC.2016.06.039
[10] Baik, J., Zohaib, M., Kim, U., Aadil, M., & Choi, M. (2019). Agricultural drought assessment based on multiple soil moisture products. Journal of Arid Environments, 167, 43–55. https://doi.org/10.1016/j.jaridenv.2019.04.007
[11] Smith, A. B., & Katz, R. W. (2013). US billion-dollar weather and climate disasters: Data sources, trends, accuracy and biases. Natural Hazards, 67(2), 387–410. https://doi.org/10.1007/s11069-013-0566-5
[12] Mishra, A. K., & Singh, V. P. (2011). Drought modeling - A review. Journal of Hydrology, 403(1–2), 157–175. https://doi.org/10.1016/j.jhydrol.2011.03.049
[13] Dalezios, N. R., Dercas, N., Spyropoulos, N. V., & Psomiadis, E. (2019). Remotely sensed methodologies for crop water availability and requirements in precision farming of vulnerable agriculture. Water Resources Management, 33(4), 1499–1519. https://doi.org/10.1007/s11269-018-2161-8
[14] AghaKouchak, A., Farahmand, A., Melton, F. S., Teixeira, J., Anderson, M. C., Wardlow, B. D., & Hain, C. R. (2015). Remote sensing of drought: Progress, challenges and opportunities. Reviews of Geophysics, 53(2), 452–480. https://doi.org/10.1002/2014RG000456
[15] Hazaymeh, K., & K. Hassan, Q. (2016). Remote sensing of agricultural drought monitoring: A state of art review. AIMS Environmental Science, 3(4), 604–630. https://doi.org/10.3934/environsci.2016.4.604
[16] West, H., Quinn, N., & Horswell, M. (2019). Remote sensing for drought monitoring & impact assessment: Progress, past challenges and future opportunities. Remote Sensing of Environment, 232, 111291. https://doi.org/10.1016/j.rse.2019.111291
[17] Sandholt, I., Rasmussen, K., & Andersen, J. (2002). A simple interpretation of the surface temperature/vegetation index space for assessment of surface moisture status. Remote Sensing of Environment, 79(2–3), 213–224. https://doi.org/10.1016/S0034-4257(01)00274-7
[18] Hu, X., Ren, H., Tansey, K., Zheng, Y., Ghent, D., Liu, X., & Yan, L. (2019). Agricultural drought monitoring using European Space Agency Sentinel 3A land surface temperature and normalized difference vegetation index imageries. Agricultural and Forest Meteorology, 279, 107707. https://doi.org/10.1016/j.agrformet.2019.107707
[19] Zhou, X., Wang, P., Tansey, K., Zhang, S., Li, H., & Wang, L. (2020). Developing a fused vegetation temperature condition index for drought monitoring at field scales using Sentinel-2 and MODIS imagery. Computers and Electronics in Agriculture, 168, 105144. https://doi.org/10.1016/j.compag.2019.105144
[20] Patel, N. R., Mukund, A., & Parida, B. R. (2022). Satellite-derived vegetation temperature condition index to infer root zone soil moisture in semi-arid province of Rajasthan, India. Geocarto International, 37(1), 179–195. https://doi.org/10.1080/10106049.2019.1704074
[21] Dalezios, N. R., Blanta, A., & Spyropoulos, N. V. (2012). Assessment of remotely sensed drought features in vulnerable agriculture. Natural Hazards and Earth System Sciences, 12(10), 3139–3150. https://doi.org/10.5194/nhess-12-3139-2012
[22] Zarco-Tejada, P. J., Rueda, C. A., & Ustin, S. L. (2003). Water content estimation in vegetation with MODIS reflectance data and model inversion methods. Remote Sensing of Environment, 85(1), 109–124. https://doi.org/10.1016/S0034-4257(02)00197-9
[23] Gao, B. (1996). NDWI—A normalized difference water index for remote sensing of vegetation liquid water from space. Remote Sensing of Environment, 58(3), 257–266. https://doi.org/10.1016/S0034-4257(96)00067-3
[24] Cheng-lin, L., & Jian-jun, W. (2008). Crop drought monitoring using MODIS NDDI over Mid-Territory of China. 2008 IEEE International Geoscience and Remote Sensing Symposium, III-883-III–886. https://doi.org/10.1109/IGARSS.2008.4779491
[25] Xiao, X., Hollinger, D., Aber, J., Goltz, M., Davidson, E. A., Zhang, Q., & Moore, B. (2004). Satellite-based modeling of gross primary production in an evergreen needleleaf forest. Remote Sensing of Environment, 89(4), 519–534. https://doi.org/10.1016/j.rse.2003.11.008

[26] Kogan, F. (2002). World droughts in the new millennium from AVHRR-based vegetation health indices. Eos, Transactions American Geophysical Union, 83(48), 557. https://doi.org/10.1029/2002EO000382
[27] Heydari, H., Valadan Zoej, M., Maghsoudi, Y., & Dehnavi, S. (2018). An investigation of drought prediction using various remote-sensing vegetation indices for different time spans. International Journal of Remote Sensing, 39(6), 1871–1889. https://doi.org/10.1080/01431161.2017.1416696
[28] Ribeiro, A. F. S., Russo, A., Gouveia, C. M., & Páscoa, P. (2019). Modelling drought-related yield losses in Iberia using remote sensing and multiscalar indices. Theoretical and Applied Climatology, 136(1–2), 203–220. https://doi.org/10.1007/s00704-018-2478-5
[29] Mu, Q., Zhao, M., Kimball, J. S., McDowell, N. G., & Running, S. W. (2013). A remotely sensed global terrestrial drought severity index. Bulletin of the American Meteorological Society, 94(1), 83–98. https://doi.org/10.1175/BAMS-D-11-00213.1
[30] Um, M.-J., Kim, Y., & Park, D. (2018). Evaluation and modification of the drought severity index (DSI) in East Asia. Remote Sensing of Environment, 209, 66–76. https://doi.org/10.1016/j.rse.2018.02.044
[31] Huang, J., Zhuo, W., Li, Y., Huang, R., Sedano, F., Su, W., Dong, J., Tian, L., Huang, Y., Zhu, D., & Zhang, X. (2020). Comparison of three remotely sensed drought indices for assessing the impact of drought on winter wheat yield. International Journal of Digital Earth, 13(4), 504–526. https://doi.org/10.1080/17538947.2018.1542040
[32] Kogan, F. N. (1995). Application of vegetation index and brightness temperature for drought detection. Advances in Space Research, 15(11), 91–100. https://doi.org/10.1016/0273-1177(95)00079-T
[33] Hao, C., Zhang, J., & Yao, F. (2015). Combination of multi-sensor remote sensing data for drought monitoring over Southwest China. International Journal of Applied Earth Observation and Geoinformation, 35, 270–283. https://doi.org/10.1016/j.jag.2014.09.011
[34] Zhang, H., Ma, J., Chen, C., & Tian, X. (2020). NDVI-Net: A fusion network for generating high-resolution normalized difference vegetation index in remote sensing. ISPRS Journal of Photogrammetry and Remote Sensing, 168, 182–196. https://doi.org/10.1016/j.isprsjprs.2020.08.010
[35] Kamble, M. V., Ghosh, K., Rajeevan, M., & Samui, R. P. (2010). Drought monitoring over India through normalized difference vegetation index (NDVI). MAUSAM, 61(4), 537–546. https://doi.org/10.54302/mausam.v61i4.911
[36] Sahoo, A. K., Sheffield, J., Pan, M., & Wood, E. F. (2015). Evaluation of the tropical rainfall measuring mission multi-satellite precipitation analysis (TMPA) for assessment of large-scale meteorological drought. Remote Sensing of Environment, 159, 181–193. https://doi.org/10.1016/j.rse.2014.11.032
[37] Liu, D., Mishra, A. K., Yu, Z., Yang, C., Konapala, G., & Vu, T. (2017). Performance of SMAP, AMSR-E and LAI for weekly agricultural drought forecasting over continental United States. Journal of Hydrology, 553, 88–104. https://doi.org/10.1016/j.jhydrol.2017.07.049
[38] Guha S, G. H. D. P. (2019). Analytical study of seasonal variability in land surface temperature with normalized difference vegetation index, normalized difference water index, normalized difference built-up index, and normalized multiband drought index. Journal of Applied Remote Sensing, 13(2), 1. https://doi.org/10.1117/1.JRS.13.024518
[39] Amalo, L. F., Hidayat, R., & Sulma, S. (2018). Analysis of agricultural drought in East Java using vegetation health index. AGRIVITA Journal of Agricultural Science, 40(1), 63-73. https://doi.org/10.17503/agrivita.v40i1.1080
[40] Prasetyo, S. Y. J., Dwi Hartomo, K., Chrismawati Paseleng, M., Chandra, D. W., & Winarko, E. (2020). Satellite imagery and machine learning for aridity disaster classification using vegetation indices. Bulletin of Electrical Engineering and Informatics, 9(3), 1149–1158. https://doi.org/10.11591/eei.v9i3.1916
[41] Sholihah, R. I., Trisasongko, B. H., Shiddiq, D., Iman, L. O. S., Kusdaryanto, S., Manijo, & Panuju, D. R. (2016). Identification of agricultural drought extent based on vegetation health indices of Landsat data: Case of Subang and Karawang, Indonesia. Procedia Environmental Sciences, 33, 14–20. https://doi.org/10.1016/j.proenv.2016.03.051
[42] Rismayatika, F., Saraswati, R., Shidiq, I. P. A., & Taqyyudin. (2020). Identification of dry areas on agricultural land using normalized difference drought index in Magetan Regency. IOP Conference Series: Earth and Environmental Science, 540(1), 012029. https://doi.org/10.1088/1755-1315/540/1/012029
[43] Dzakiyah, I. F., Saraswati, R., & Pamungkas, F. D. (2022). The potential of agricultural land drought using normalized difference drought index in Ciampel Subdistrict Karawang Regency. International Journal on Advanced Science, Engineering and Information Technology, 12(3), 908. https://doi.org/10.18517/ijaseit.12.3.13261
[44] Du, T. L. T., Bui, D. Du, Nguyen, M. D., & Lee, H. (2018). Satellite-based, multi-indices for evaluation of agricultural droughts in a highly dynamic tropical catchment, Central Vietnam. Water, 10(5), 659. https://doi.org/10.3390/w10050659

[45] Xie, F., & Fan, H. (2021). Deriving drought indices from MODIS vegetation indices (NDVI/EVI) and land surface temperature (LST): Is data reconstruction necessary? International Journal of Applied Earth Observation and Geoinformation, 101, 102352. https://doi.org/10.1016/j.jag.2021.102352
[46] Rezaeianzadeh, M., Stein, A., & Cox, J. P. (2016). Drought forecasting using Markov chain model and artificial neural networks. Water Resources Management, 30(7), 2245–2259. https://doi.org/10.1007/s11269-016-1283-0
[47] Lohani, V. K., & Loganathan, G. V. (1997). An Early warning system for drought management using the Palmer drought index. Journal of the American Water Resources Association, 33(6), 1375–1386. https://doi.org/10.1111/j.1752-1688.1997.tb03560.x
[48] Iqbal, M., & Naveed, A. (2016). Forecasting inflation: Autoregressive integrated moving average model. European Scientific Journal, ESJ, 12(1), 83. https://doi.org/10.19044/esj.2016.v12n1p83
[49] Zhang, Y., Yang, H., Cui, H., & Chen, Q. (2020). Comparison of the ability of ARIMA, WNN and SVM models for drought forecasting in the Sanjiang Plain, China. Natural Resources Research, 29(2), 1447–1464. https://doi.org/10.1007/s11053-019-09512-6
[50] Godfrey, G. A., & Powell, W. B. (2000). Adaptive estimation of daily demands with complex calendar effects for freight transportation. Transportation Research Part B: Methodological, 34(6), 451–469. https://doi.org/10.1016/S0965-8564(99)00032-4
[51] Valipour, M., Banihabib, M. E., & Behbahani, S. M. R. (2013). Comparison of the ARMA, ARIMA, and the autoregressive artificial neural network models in forecasting the monthly inflow of Dez dam reservoir. Journal of Hydrology, 476, 433–441. https://doi.org/10.1016/j.jhydrol.2012.11.017
[52] Valipour, M. (2015). Long-term runoff study using SARIMA and ARIMA models in the United States. Meteorological Applications, 22(3), 592–598. https://doi.org/10.1002/met.1491
[53] Nuf'a, H., Limantara, L. M., & Soetopo, W. (2016). Optimasi air waduk gondang dengan metode dinamik deterministik. Jurnal Teknik Pengairan, 7(1), 25–36.
[54] Giovanni, N. (2018). Identifikasi kekeringan padi sawah dengan indeks NDDI dan VHI dari Citra Landsat 8 di Kabupaten Subang. Thesis. Institut Pertanian Bogor.
[55] Khampeera, A., Yongchalermchai, C., & Techato, K. (2017). Drought monitoring using drought indices and GIS techniques in Kuan Kreng Peat Swamp, Southern Thailand. Walailak Journal of Science and Technology (WJST), 15(5), 357–370. https://doi.org/10.48048/wjst.2018.2723
[56] Dobri, R.-V., Sfîcă, L., Amihăesei, V.-A., Apostol, L., & Ţîmpu, S. (2021). Drought extent and severity on arable lands in Romania derived from normalized difference drought index (2001–2020). Remote Sensing, 13(8), 1478. https://doi.org/10.3390/rs13081478
[57] Trinh, L. H., & Vu, D. T. (2019). Application of remote sensing technique for drought assessment based on normalized difference drought index, a case study of Bac Binh district, Binh Thuan province (Vietnam). Russian Journal of Earth Sciences, 19(2), 1–9. https://doi.org/10.2205/2018ES000647
[58] Cryer, J. D. (1986). Time Series Analysis. PWS-KENT Publishing Company.
[59] Farsi, M., Hosahalli, D., Manjunatha, B. R., Gad, I., Atlam, E.-S., Ahmed, A., Elmarhomy, G., Elmarhoumy, M., & Ghoneim, O. A. (2021). Parallel genetic algorithms for optimizing the SARIMA model for better forecasting of the NCDC weather data. Alexandria Engineering Journal, 60(1), 1299–1316. https://doi.org/10.1016/j.aej.2020.10.052
[60] Etuk, E. H., & Mohamed, T. M. (2014). Time series analysis of monthly rainfall data for the Gadaref rainfall station, Sudan, by Sarima Methods. International Journal of Scientific Research in Knowledge, 320–327. https://doi.org/10.12983/ijsrk-2014-p0320-0327
[61] Dabral, P. P., & Murry, M. Z. (2017). Modelling and forecasting of rainfall time series using SARIMA. Environmental Processes, 4(2), 399–419. https://doi.org/10.1007/s40710-017-0226-y
[62] Xue, J., & Su, B. (2017). Significant remote sensing vegetation indices: A review of developments and applications. Journal of Sensors, 2017, 1–17. https://doi.org/10.1155/2017/1353691
[63] Naif, S. S., Mahmood, D. A., & Al-Jiboori, M. H. (2020). Seasonal normalized difference vegetation index responses to air temperature and precipitation in Baghdad. Open Agriculture, 5(1), 631–637. https://doi.org/10.1515/opag-2020-0065
[64] Pervez, M. S., & Brown, J. F. (2010). Mapping irrigated lands at 250-m scale by merging MODIS data and national agricultural statistics. Remote Sensing, 2(10), 2388–2412. https://doi.org/10.3390/rs2102388
[65] Hazaymeh, K., & Hassan, Q. K. (2017). A remote sensing-based agricultural drought indicator and its implementation over a semi-arid region, Jordan. Journal of Arid Land, 9(3), 319–330. https://doi.org/10.1007/s40333-017-0014-6